Annals of Nuclear Cardiology Vol. 6 No. 1 95–98

REVIEW ARTICLE—JSNC TECHNOLOGIST AWARD

Simulation Study of High-sensitivity Cardiac-dedicated PET Systems with Different Geometries

Go Akamatsu, PhD, Hideaki Tashima, PhD, Yuma Iwao, PhD, Miwako Takahashi, MD, PhD, Eiji Yoshida, PhD and Taiga Yamaya, PhD

Received: November 26, 2019/Revised manuscript received: March 18, 2020/Accepted: March 21, 2020
J-STAGE advance published: July 30, 2020

Abstract

Noninvasive quantification of myocardial blood flow with PET is a vital tool for detecting and monitoring of coronary artery disease. However, current standard cylindrical PET scanners are not optimized for cardiac imaging because they are designed mainly for whole-body imaging. In this study, we proposed two compact geometries, the elliptical geometry and the D-shape geometry, for cardiac-dedicated PET systems. We then evaluated their performance compared with a whole-body-size cylindrical geometry by using the Geant4 Monte Carlo simulation toolkit. In the simulation, an elliptical water phantom was scanned for 10-sec, and we calculated the sensitivity and the noise-equivalent count rate (NECR). Subsequently, a digital chest phantom was scanned for 30-sec and the coincidence data were reconstructed by in-house image reconstruction software. We evaluated the image noise in the liver region and the contrast recoveries in the heart region. Even with the limited number of detectors, the proposed compact geometries showed higher sensitivity than the whole-body geometry. The D-shape geometry achieved 47% higher NECR and 44% lower image noise compared with the whole-body cylindrical geometry. However, the contrasts in the hot area obtained by the proposed compact geometries were not as good as that obtained by the whole-body cylindrical geometry. There was no considerable difference in image quality between the elliptical geometry and the D-shape geometry. In conclusion, the compact geometries we have proposed are promising designs for a high-sensitivity and low-cost cardiac-dedicated PET system. A further study using a defect phantom model is required to evaluate the contrast of cold areas.

Keywords: Cardiac-dedicated PET, Instrumentation, PET, Simulation
Ann Nucl Cardiol 2020; 6 (1): 95–98

Coronary artery disease (CAD) is one of the leading causes of death world-wide. Noninvasive quantification of myocardial blood flow with SPECT or PET is a vital tool for detecting and monitoring CAD. Compared with SPECT, PET can provide better image quality and more accurate quantification, and allow dynamic first-pass imaging (1). A novel promising tracer, ^{18}F-flurpiridaz, has been developed and its phase III trial is going on (2). It is expected that the demand for cardiac PET imaging will increase hereafter. However, current standard PET scanners are not optimized for cardiac imaging because they are designed mainly for whole-body imaging. A more compact geometry can increase the sensitivity and would be suitable for cardiac imaging.

In this study, we proposed two compact geometries for cardiac-dedicated PET systems, and evaluated their performance compared with a whole-body-size cylindrical geometry by using a simulation.

Materials and methods

Proposed geometries and system specifications

Using the Geant4 simulation toolkit (3, 4), we modeled three different PET systems: a whole-body-size cylindrical geometry, an elliptical geometry and a D-shape geometry (Figure 1). Although the D-shape geometry itself has been already studied (5), the D-shape proposed in this study has a smaller diameter to fit a torso closely. Specifications of the

doi: 10.17996/anc.20-00114

National Institute of Radiological Sciences, National Institutes for Quantum and Radiological Science and Technology (NIRS-QST), Chiba, Japan.

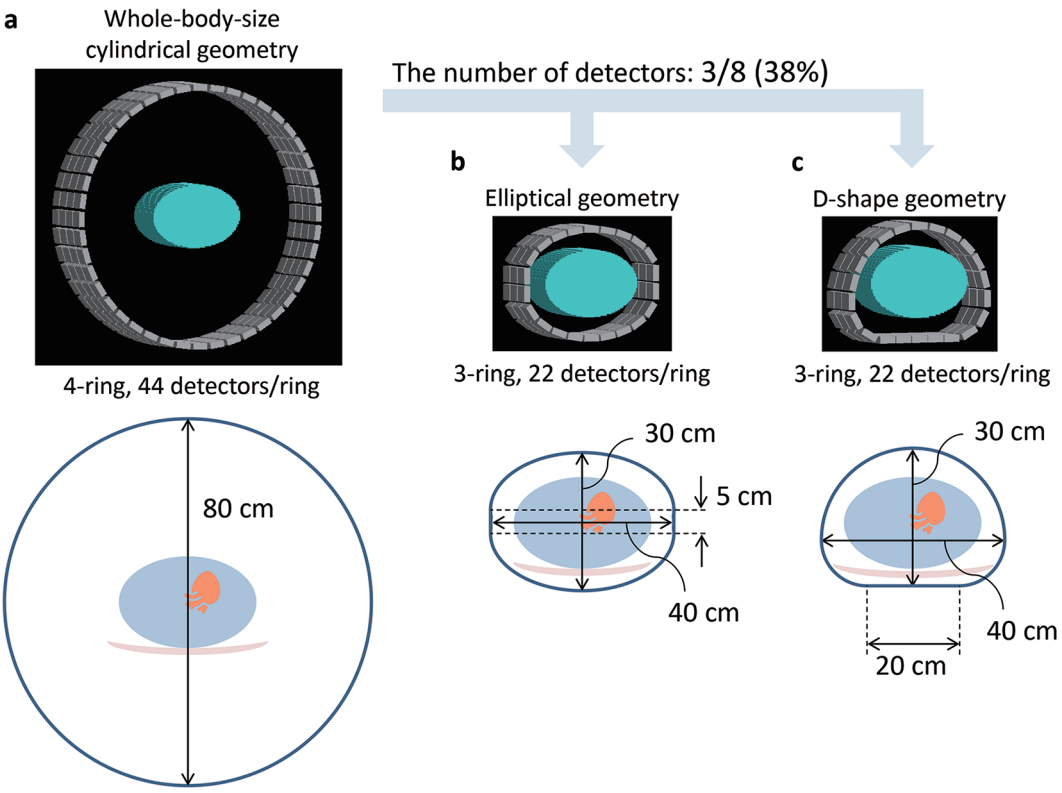

Figure 1　Detector arrangements of the simulated PET systems with the whole-body-size cylindrical geometry (**a**), the elliptical geometry (**b**), and the D-shape geometry (**c**).

Table 1　Simulation parameters for the three geometries

	Cylindrical geometry	Elliptical geometry	D-shape geometry
Scintillation crystals	LYSO	LYSO	LYSO
Size of crystals	$4.0\times4.0\times20$ mm^3	$4.0\times4.0\times20$ mm^3	$4.0\times4.0\times20$ mm^3
Number of crystals per detector	12×12	12×12	12×12
Number of detector rings	4	3	3
Number of detectors	176	66	66
TOF coincidence timing resolution	300 ps	300 ps	300 ps
Energy resolution	12%	12%	12%
Energy window	400-600 keV	400-600 keV	400-600 keV
Coincidence time window	6 ns	4 ns	4 ns

TOF: time-of-flight, LYSO: Lutetium yttrium oxyorthosilicate

simulated systems are shown in Table 1. These specifications are based on realizable performance (6). For the whole-body-size geometry, the larger coincidence time window of 6 ns was used in consideration of collecting all true coincidence counts. In each detector block, a paralyzable dead time of 1 μs was applied to a single event.

Sensitivity and noise equivalent count ratio (NECR)

The elliptical water phantom was placed on the central field-of-view (Figure 1). The long axis was 30 cm, the short axis was 20 cm and the length was 15 cm. The size and shape of the phantom mimicked a human chest. The water phantom was uniformly filled with an ^{18}F activity of 10 MBq. Sensitivity was measured as the ratio of true coincidence count and decay count. At the fixed activity of 10 MBq, we calculated noise-equivalent count ratio (NECR) using the following equation:

$$NECR=\frac{T^2}{T+S+R}$$

where T, S, and R are the true, scatter, and random coincidence count rates, respectively.

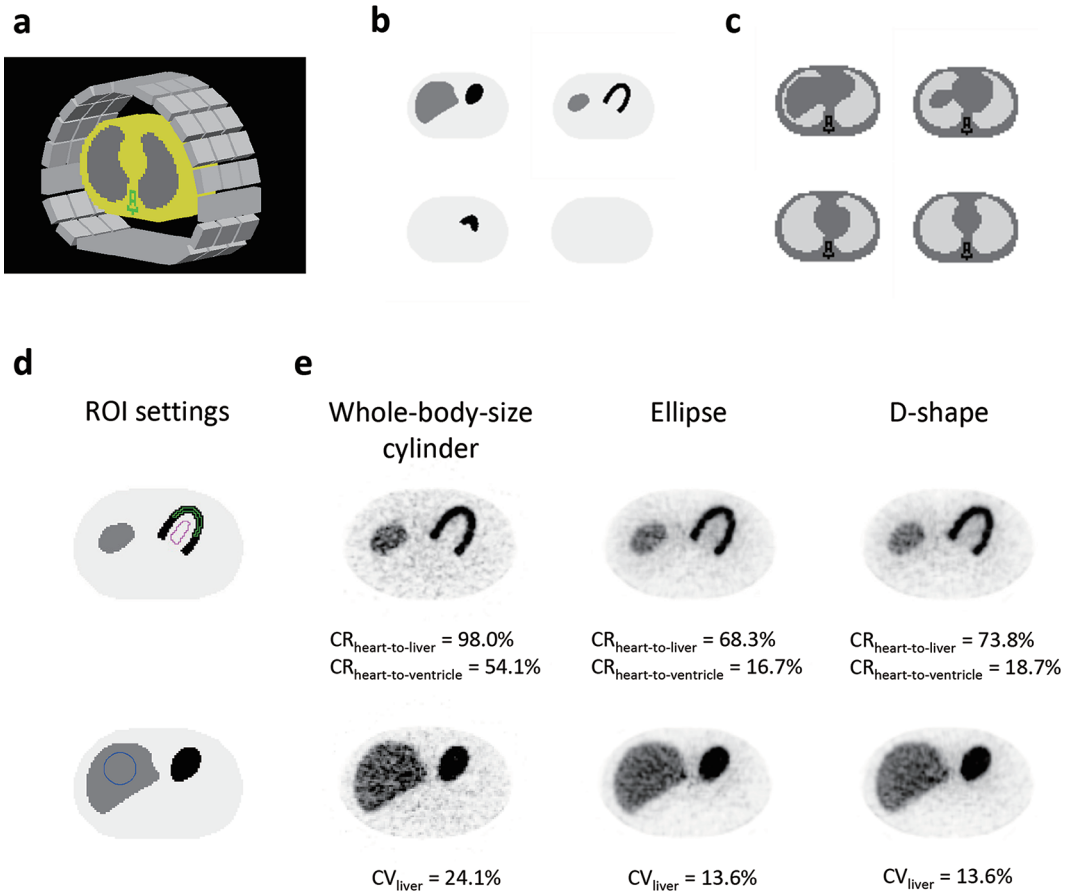

Figure 2 Simulation setup (D-shape geometry) (**a**) and four representative slices of the activity map (**b**) and attenuation map (**c**), and ROI settings (**d**) for the digital chest phantom. PET images and their $CR_{heart\text{-}to\text{-}liver}$, $CR_{heart\text{-}to\text{-}ventricle}$ and CV_{liver}, obtained by the three different geometries (**e**).

Image quality evaluation

The digital chest phantom provided by the Japanese Society of Nuclear Medicine was used for image quality evaluation (Figure 2a) (7). Activity of ^{18}F was 10 MBq in total. The activity ratio of heart, liver, and background was 20:10:1 (Figure 2b). The attenuation coefficient map included bone, lung, and soft tissue (Figure 2c). Scan duration was 30 seconds, assuming dynamic imaging. Coincidence data were reconstructed by the 3-dimensional (3D) ordered-subsets expectation-maximization (OSEM) algorithm with 3 iterations and 8 subsets. Normalization, attenuation, scatter and singles-based random corrections were included in the reconstruction process. The image matrix size was $128 \times 128 \times 64$ with a 3.0 mm isotropic voxel. A 5-cm-diameter circular region-of-interest (ROI) was placed on the liver in three axial slices (Figure 2d). For image noise evaluation, we measured a coefficient of variation (CV) in the ROIs as follows:

$$CV_{liver} = \frac{SD_{liver}}{C_{liver}} \times 100\ (\%)$$

where SD_{liver} is the standard deviation of the ROI values and C_{liver} is the average of the ROI values. In addition, ROIs were manually placed on the heart and ventricle in three axial slices as shown in Figure 2d. We measured the contrast recoveries (CRs) as follows:

$$CR_{heart\text{-}to\text{-}liver} = \frac{C_{heart}/C_{liver} - 1}{a_{heart}/a_{liver} - 1} \times 100\ (\%)$$

$$CR_{heart\text{-}to\text{-}ventricle} = \frac{C_{heart}/C_{ventricle} - 1}{a_{heart}/a_{ventricle} - 1} \times 100\%$$

where C_{heart} and $C_{ventricle}$ are the averages of the ROI values on the heart and ventricle, and a_{heart} and a_{liver} are the true values on the heart and liver, respectively. The $a_{heart/aliver}$ and $a_{heart}/a_{ventricle}$ are 2 and 20, respectively.

Results

The sensitivities of the whole-body cylindrical geometry, the elliptical geometry, and the D-shape geometry were 0.56%, 0.94% and 0.96%, respectively. The corresponding NECRs were 33.1, 47.7, and 48.6 kcps. The D-shape geometry showed the highest sensitivity and the highest NECR.

PET images of the digital chest phantom and those $CR_{heart\text{-}to\text{-}liver}$, $CR_{heart\text{-}to\text{-}ventricle}$ and CV_{liver} are shown in Figure 2e. The compact elliptical and D-shape geometries achieved a superior CV_{liver} compared to the whole-body-size cylindrical

geometry. On the other hand, the $CR_{heart\text{-}to\text{-}liver}$ and $CR_{heart\text{-}to\text{-}ventricle}$, obtained by the compact geometries were not as good as that obtained by the whole-body-size cylindrical geometry.

Discussion

We proposed two compact geometries for cardiac-dedicated PET systems and carried out their Monte Carlo simulation. For the compact geometries, the number of detectors was 3/8 (62.5% reduction) compared to the whole-body cylindrical geometry. Production cost and system size for the former two geometries can be reduced compared with the standard whole-body cylindrical geometry.

The compact D-shape geometry achieved 47% higher NECR and 44% lower image noise (CV_{liver}) compared with the whole-body cylindrical geometry. Even with the limited number of detectors, the proposed compact geometries showed higher sensitivity than the whole-body cylindrical geometry. These compact geometries might enable more accurate dynamic myocardial imaging. However, the contrast recoveries ($CR_{heart\text{-}to\text{-}liver}$ and $CR_{heart\text{-}to\text{-}ventricle}$) for these compact geometries was not as good as that for the whole-body cylindrical geometry. The reason for this degradation would be parallax error. The effect of parallax error is bigger as the detector ring diameter is decreased while the sensitivity is increased (8). A further investigation using a point source is needed to clarify the effect of parallax error for these compact geometries. A detector with depth-of-interaction (DOI) measurement capability is preferable to address this issue. In addition, as we simulated the only one crystal size, further simulations using various crystal sizes and detector configurations are needed to investigate a suitable detector configuration for cardiac imaging. The combination of a compact geometry and a smaller scintillation crystal might achieve higher contrast with acceptable noise level because of its higher sensitivity.

There was no considerable difference in image quality between the elliptical geometry and the D-shape geometry. In this work, we only evaluated image noise levels and the image contrast in hot areas on reconstructed PET images. For cardiac PET imaging, the image contrast of defect regions (cold contrast) is critical to detect myocardial ischemia. Next, we need to evaluate the contrast of cold areas using a defect phantom model.

Conclusion

The compact geometries we have proposed are promising designs for a high-sensitivity and low-cost cardiac-dedicated PET system. A further study using a defect phantom model is required in order to evaluate the contrast of cold areas.

Acknowledgments

None.

Sources of funding

This study was supported by QST President's Strategic Grant (Exploratory Research).

Conflicts of interest

No conflicts of interest are disclosed.

Reprint requests and correspondence:
Go Akamatsu, PhD
National Institute of Radiological Sciences, National Institutes for Quantum and Radiological Science and Technology (NIRS-QST), 4-9-1 Anagawa, Inage-ku, Chiba 263-8555, Japan
E-mail: akamatsu.go@qst.go.jp

References

1. Berman DS, Germano G, Slomka PJ. Improvement in PET myocardial perfusion image quality and quantification with flurpiridaz F 18. J Nucl Cardiol 2012; 19: S38–45.
2. Werner RA, Chen X, Rowe SP, Lapa C, Javadi MS, Higuchi T. Moving into the next era of PET myocardial perfusion imaging: introduction of novel ^{18}F-labeled tracers. Int J Cardiovasc Imaging 2019; 35: 569–77.
3. Agostinelli S, Allison J, Amako K, et al. Geant4—a simulation toolkit. Nucl Instrum Methods Phys Res A 2003; 506: 250–303.
4. Tashima H, Yoshida E, Akamatsu G, Yamaya T. Development of an imaging simulation framework enabling modelling of PET scanners with arbitrary detector arrangement. In: The 115th Annual Meeting of the Japan Society of Medical Physics, Yokohama, 2018.
5. Ahmed AM, Tashima H, Yamaya T. Simulation study of a D-shape PET scanner for improved sensitivity and reduced cost in whole-body imaging. Phys Med Biol 2017; 62: 4107–17.
6. Yoshida E, Tashima H, Akamatsu G, et al. 245 ps-TOF brain-dedicated PET prototype with a hemispherical detector arrangement. Phys Med Biol 2020; 65: 145008.
7. Japanese Society of Nuclear Medicine. Digital chest phantom. Available at: https://member.jsnm.org/portal/digital-phantom.html.
8. Mohammadi I, Castro IFC, Correia PMM, Silva ALM, Veloso JFCA. Minimization of parallax error in positron emission tomography using depth of interaction capable detectors: methods and apparatus. Biomed Phys Eng Express 2019; 5: 062001.